ADVANCED MATERIALS

DOI: 10.1002/adma.200801090

Stop-Flow Lithography of Colloidal, Glass, and Silicon Microcomponents**

By *Robert F. Shepherd, Priyadarshi Panda, Zhihao Bao, Kenneth H. Sandhage, T. Alan Hatton, Jennifer A. Lewis,** and *Patrick S. Doyle**

The assembly of oxide and non-oxide microcomponents from colloidal building blocks is central to a broad array of applications, including sensors, optical devices, and microelectromechanical systems (MEMS), as well as to fundamental studies of granular materials. Progress in these areas has been hindered by the availability of colloidal microcomponents of precisely tailored size, shape, and composition. Hence, there is tremendous interest in developing new patterning methods for creating precisely tailored microcomponents composed of colloidal building blocks, amorphous or polycrystalline oxides, and silicon. For example, colloidal-based microcomponents produced in simple non-spherical shapes, such as discoid, triangular, cuboid, and rectangular, may serve as novel granular feedstock for ceramics,[1,2] optical display technologies[3] and pharmaceuticals.[4,5] Traditional methods for producing colloidal granules, such as fluid bed granulation,[6] high shear mixer granulation,[7] and spray drying,[2] do not provide adequate control over granule size, shape, or composition. Equally important is the need to create porous and dense oxide and non-oxide microcomponents for functional devices ranging from micro-mixers and heat exchangers[8,9] to MEMS.[10–14] Although several fabrication methods have been recently introduced, including lithography, electroplating and molding (LIGA),[15,16] micro-extrusion,[17] micro-injection molding,[18,19] micro-stereolithography,[20,21] and micro- electro-discharge machining,[22] each lacks the materials flexibility or rapid assembly times desired for many applications.

Microfluidic assembly techniques provide a new platform for creating novel polymer particles from photopolymerizable resins[23–26] and hydrogels[27,28] as well as colloidal granules.[29] In most cases, the particles (or granules) are produced by co-flowing immiscible liquids through a microfluidic device that induces droplet break off yielding one particle at a time.[30,31] Due to surface-tension effects, only spherical shapes or deformations thereof are readily produced. Another technique for the production of polymeric microparticles, forms polystyrene microbeads into higher order assemblies via microfluidic patterning and thermal fusion.[32] By contrast, stop-flow lithography (SFL)[33] enables a rich array of simple and complex shapes to be produced, in parallel, at production rates in excess of 10^6 min^{-1}. SFL employs microscope projection photolithography[34] to create patterned structures within a microfluidic device, eliminating the need for clean room conditions. To date, SFL has been used for applications such as biomolecular analysis,[35] assembly of Janus particles[36] and interference lithography.[37] Here, for the first time, we report the assembly of colloidal granules and microcomponents in the form of microgear, triangular, discoid, cuboid, and rectangular shapes using SFL as well as demonstrate pathways by which they can be transformed into both porous and dense oxide and non-oxide structures.

We demonstrate this novel assembly method by first designing a model colloidal suspension capable of being rapidly polymerized via projection lithography within a microfluidic device. The system is composed of silica microspheres suspended in a mixture of dimethyl sulfoxide (DMSO) and water at a volume fraction, ϕ_{silica}, of 0.5. The suspension also contains acrylamide monomer ($\phi_{acrylamide} = 0.08$), a cross-linking agent (monomer:crosslinking agent ratio of 4:1 by weight), and photoinitiator ($\phi_{initiator} = 0.03$). This photopolymerizable colloidal suspension must exhibit limited scattering and absorption of the incident ultraviolet light to ensure high resolution of the as-patterned features. Aqueous silica suspensions are opaque due to the refractive index difference between silica ($n = 1.46$) and water ($n = 1.33$). By adding an appropriate amount of DMSO ($n = 1.48$), the colloid and fluid phases are index-matched thereby minimizing scattering from the suspended particles.

The SFL setup utilized in the present work is illustrated in Figure 1a. Patterned microcomponent(s) are formed by projecting ultraviolet light through a photomask inserted into

[*] Prof. J. A. Lewis, R. F. Shepherd
Department of Material Science and Engineering, University of Illinois, U-C
1304 W Green St., Urbana, IL 61801 (USA)
E-mail: jalewis@uiuc.edu

Prof. P. S. Doyle, P. Panda, Prof. T. A. Hatton
Department of Chemical Engineering, Massachusetts Institute of Technology
77 Massachusetts Avenue, Cambridge, MA 02139 (USA)
E-mail: pdoyle@mit.edu

Z. Bao, Prof. K. H. Sandhage
School of Material Science and Engineering, Georgia Institute of Technology
771 Ferst Drive, Atlanta, GA 30332 (USA)

[**] R. F. S and P. P contributed equally to this work. J. A. L., P. S. D., and K. H. S. designed the research; R. F. S., P. P., and Z. B. performed the research, R. F. S., P. P., J. A. L., and P. S. D. wrote the paper. This material is based on work supported by the National Science Foundation (DMR-0652424, CTS-0120978 and CTS-0304128) and the Air Force Office of Scientific Research (FA9550-05-1-0092). The authors thank A. Deconinck for software development, K. Erickson, S. M. Menke, A. Cote, and A. Balducci for useful discussions, and M. McConney and S. MacLaren for assistance with AFM.

© 2008 WILEY-VCH Verlag GmbH & Co. KGaA, Weinheim

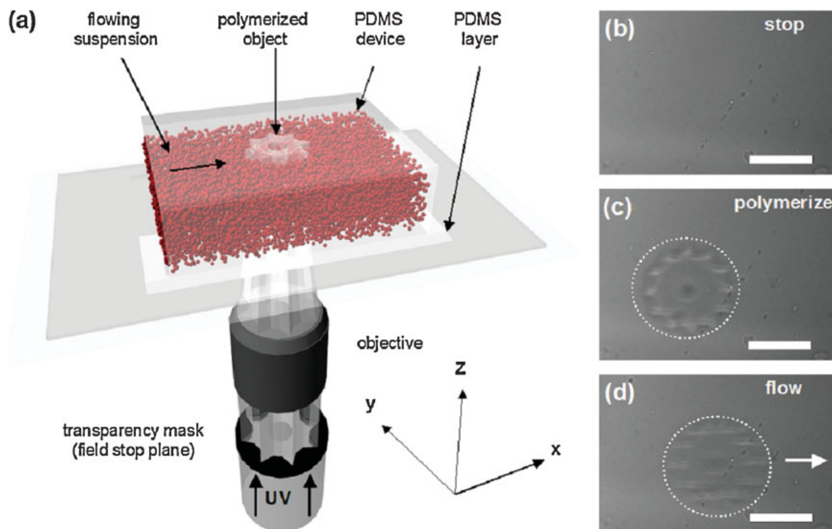

Figure 1. a) Schematic illustration of stop flow lithography (SFL) system, where a photocurable, index-matched silica-acrylamide suspension is flowed through a PDMS microchannel. Microcomponents are patterned by b) bringing the suspension to a complete stop within the microchannel, then c) illuminating a defined volume of the suspension with UV light to induce photopolymerization, followed by d) ejection of the as-patterned component through re-initiation of suspension flow. This process is repeated until the desired number of microcomponents is formed, at rates exceeding 10^3 min^{-1}. [Scalebars (b–d) are 100 μm.]

the field stop of an inverted microscope. Microcomponent fabrication involves the stop-polymerize-flow sequence[33] captured in optical images shown in Figure 1b–d. Figure 1b shows an image of a suspension-filled microchannel prior to UV polymerization. The suspension is transparent due to its index-matched state. Figure 1c is acquired immediately after photopolymerization and shows a colloidal microgear that consists of a polyacrylamide network filled with silica microspheres and the solvent mixture. The modest change in refractive index upon polymerization enables one to visualize the as-patterned structure within the microchannel. Finally, Figure 1d shows the microgear as it accelerates in response to the onset of an applied pressure within the microchannel. A video of microgear formation is presented as Supporting Information.

To minimize microcomponent shrinkage during drying, we utilize suspensions with high solids loading ($\phi_{\text{silica}} = 0.5$) that are capable of flowing through the SFL device without clogging. The photopolymerizable suspensions exhibit Newtonian flow behavior when $\phi_{\text{silica}} < 0.35$ (data not shown). At $\phi_{\text{silica}} \sim 0.35$, there is a transition to shear thinning behavior, which becomes more pronounced with increasing ϕ_{silica} (Fig. 2a). This behavior facilitates their flow through the SFL device at modest applied pressures.

We carried out particle tracking measurements for index-matched suspensions of varying colloidal volume fraction to obtain centerline velocities (Fig. 2b). We estimate characteristic shear rates, which range from 50 to 262 s^{-1}, for colloidal suspensions of $\phi_{\text{silica}} = 0.5$–$0.35$, respectively, by dividing the maximum centerline velocity by half the microchannel height. Over this shear rate range, each suspension can be approximated to first order as a Newtonian fluid (Fig. 2a). The centerline velocity at the exit of a low aspect ratio (H/W<1) deformable PDMS microchannel is estimated by:[33,38]

$$V(L) = \frac{H^3 E}{32 W \eta L}\left[\left(1 + \frac{PW}{EH}\right)^4 - 1\right] \quad (1)$$

where η is the viscosity, L is the microchannel length, W is the microchannel width, E is the Young's modulus of PDMS (1 MPa), and H is the microchannel height. These estimated velocities are in good agreement with the measured maximum centerline velocities (see Supporting Information).

SFL consists of three distinct steps — stop, polymerize, and flow — repeated in a cyclical fashion;[33] hence, the times required to stop flow (t_{stop}), polymerize ($t_{\text{polymerize}}$), and expel the patterned components (t_{flow}) are key experimental parameters. We determine the values for t_{stop}, which range from 100 to 300 ms for colloidal suspensions of $\phi_{\text{silica}} = 0.5$–$0.35$, respectively, from the particle tracking data shown in Figure 2b. In our experiments, we utilize a value of

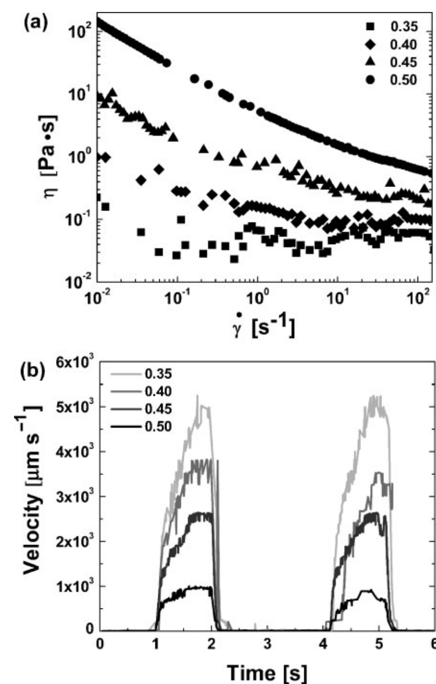

Figure 2. a) Apparent viscosity as a function of shear rate for index-matched, silica-acrylamide suspensions of varying colloid volume fraction. b) Centerline velocities for increasing solids loadings of colloidal silica within a 40 μm microchannel.

© 2008 WILEY-VCH Verlag GmbH & Co. KGaA, Weinheim

300 ms for t_{stop}, which is sufficient to ensure complete cessation of suspension flow prior to polymerization. We employ values of $t_{polymerize}$ that vary from ~200–400 ms depending on the mask design, which enable microcomponents to be patterned with precise control over shape and size. Finally, a t_{flow} value of 400 ms is used, which is sufficient to expel the patterned microcomponent from the field of view thereby preventing its double exposure.

To demonstrate the flexibility of this patterning technique, we produce colloidal microcomponents in both simple and complex shapes (Fig. 3). Specifically, we assemble microcomponents with geometries that vary from triangular, cuboid, discoid and rectangular shapes to more complicated geometries, such as microgears, with uniform sizes that range from 20 μm to 300 μm in maximum dimension. Microcomponents composed of simple geometric forms are polymerized for shorter times, because they are able to withstand the modest deformation that occurs during ejection from the microchannel. By contrast, the complex microgears require the longest $t_{polymerize}$ (400 ms) to produce rigid structures that maintain their shape during ejection. Because the microcomponents remain immersed in an index-matched solution, they appear translucent in the optical images depicted in Figure 3. The microcomponent production rates for the 2×2 and 4×1 photomask arrays are approximately 240 min^{-1} for simple shapes and 200 min^{-1} for gears. These rates can be enhanced by more than an order of magnitude by using a photomask with a larger array (e.g., see Supporting Information for video of cuboid formation using a 9×10 array).

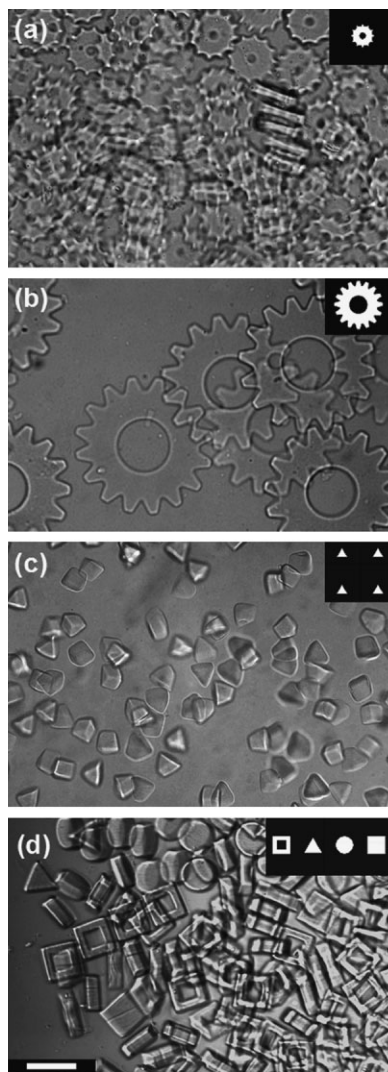

Figure 3. Optical images of colloidal microcomponents formed via SFL using the corresponding mask shown in each inset: a) small microgears formed in a 30 μm thick microchannel, b) large microgears formed in a 55 μm thick microchannel, c) equilateral triangles formed in a 60 μm thick microchannel, and d) an array of disk, cube, triangular, and rectangular microcomponents formed in a 40 μm thick microchannel. [Scalebar is 100 μm.]

We investigate the distribution of colloidal microspheres within the polymerized microcomponents using a combination of confocal laser scanning microscopy, CLSM,[39] and scanning electron microscopy (SEM). Figure 4a shows a confocal image (*x–y* scan) acquired at depth of 20 μm into a representative microgear in which 10% of the silica microspheres contain fluorescent cores. Both the *x–y* and *x–z* scans reveal that the microspheres are randomly distributed throughout the microcomponent. A full 3D reconstruction of this microgear, consisting of a series of *x–y* slices stacked together, is presented as Supporting Information. From this data, we find that the microgear thickness is approximately 50 μm. Since, in this case, photopolymerization occurred within a 55 μm deep microchannel; we believe that inhibition layers no more than a few micrometers thick form at the suspension-microchannel interfaces. Their presence facilitates microcomponent ejection once suspension flow is reinitiated. Importantly, the colloidal microgears maintain their shape after being harvested from the microfluidic device and dried, as shown in the SEM images provided in Figure 4b and c. The tilted image (Fig. 4b) clearly

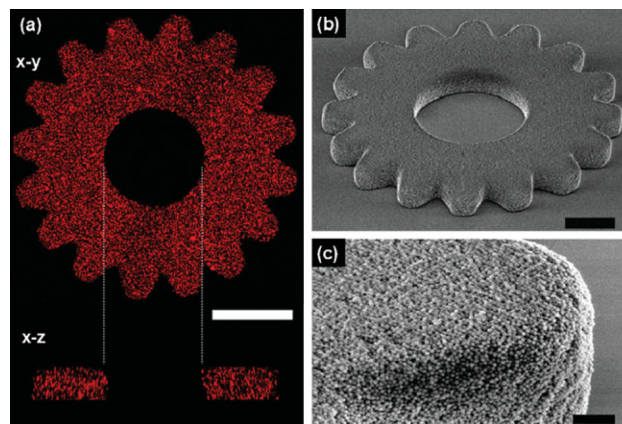

Figure 4. a) Confocal image (top, x-y plane and bottom, *x–z* plane) of patterned colloidal microgear (*x–y* scan acquired at $z = 20$ μm) in an index-matched solution. b) SEM image of a dried colloidal microgear composed of (c) densely packed silica microparticles. [Scalebars for (a)–(c) are 100 μm, 50 μm, and 5 μm, respectively.]

© 2008 WILEY-VCH Verlag GmbH & Co. KGaA, Weinheim

demonstrates that the photomask features can be replicated with a high degree of precision, while the corresponding high magnification view reveals that the colloidal microspheres are densely packed together with a final solids volume fraction of 0.62 based on optical micrographs and assuming isotropic shrinkage. We have determined the dried inner and outer gear radii to be $95 \pm 3\,\mu m$ and $225 \pm 3\,\mu m$, respectively. Additionally, through the formation of an array of microcomponents of decreasing size, we find that the minimum microcomponent feature size is approximately $8\,\mu m$ (see Supporting Information).

To enhance their structural integrity, the colloidal microgears are transformed into fully dense, glassy silica microgears by sintering at 1150 °C for 3–10 h. SEM images of a sintered glass microgear are shown in Figure 5a and b. During densification, the microgear undergoes significant radial shrinkage (~25%) resulting in the final dimensions of $71 \pm 1\,\mu m$ (inner radius) and $164 \pm 4\,\mu m$ (outer radius). Because the microcomponents are sintered on a transparent sapphire window, we can also image them via transmitted light microscopy. After sintering at 1150 °C for 3 h, the microgears are translucent. However, their surface remains rough on the size scale of the individual microsphere building blocks. At longer hold times (~10 h), the surface of the microgears becomes smooth. Their root-mean-squared (rms) surface roughness is approximately 6 nm, as determined by atomic force microscopy (Fig. 5c).

Porous silica microgears are produced by partial sintering at 1150 °C for 1 h, as shown in Figure 5d and e. These microcomponents are mechanically stable and can be readily handled. Their rms surface roughness is ~130 nm (Fig. 5f) due to the significant amount of interconnected porosity, 23 vol%, that is retained after heat treatment. This porosity aids their transformation to porous silicon microcomponents via magnesiothermic reduction.[40] In this process, the silica microgears are heated to 850 °C for 2.5 h in the presence of magnesium gas volatilized from Mg_2Si powder to promote the following reaction:

$$2Mg(g) + SiO_2(s) \rightarrow 2MgO(s) + Si(s) \qquad (2)$$

The MgO/Si composite generated by this reaction retains its 3D shape and porous features. The MgO/Si composite replicas are then immersed in a hydrochloric acid solution for 4 h to selectively dissolve the oxide phase yielding the desired porous silicon microgear replicas shown in Figure 5g and h. Energy dispersive x-ray analysis, EDX, reveals the presence of a strong silicon peak with a minimal oxygen peak (Fig. 5i). The resulting silicon replicas contain two distinct pore size distributions, one associated with the interstices between the partially sintered silica microspheres and the other associated with the "ghost" microspheres on a finer scale, where each microsphere contains 65 v/o interior porosity based on the assumption of complete conversion to silicon and removal of MgO. These porosities, combined with the 5% volumetric increase observed during the microcomponent conversion process, result in a final silicon volume fraction of 0.27. Note, the silicon content could be enhanced significantly through an additional process, such as chemical vapor deposition.[10] The rms surface roughness of the porous silicon microgears is 118 nm, in good agreement with the surface roughness of the porous silica structures from which they are replicated. These values scale with the colloid size; hence, further improvements are possible by simply reducing the mean diameter of the colloidal building blocks utilized in suspension.

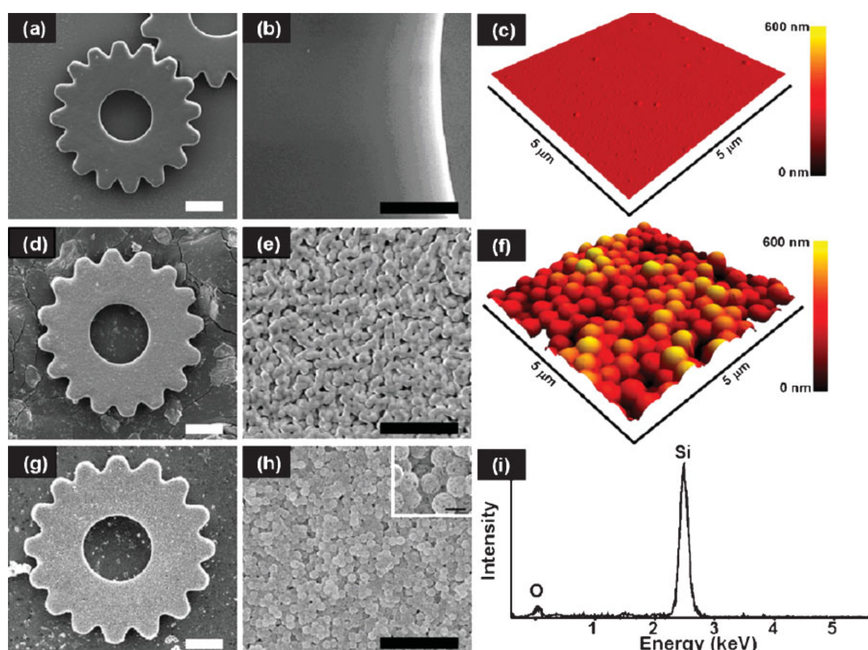

Figure 5. a) SEM micrographs of a glassy silica microgear fully densified at 1150 °C for 10 h, which is composed of b) a smooth surface and dense interior (not shown), as demonstrated by c) AFM surface reconstruction, d) SEM micrographs of a porous silica microgear partially densified at 1150 °C for 1 h, which is composed of e) a porous network of fused silica microspheres, with f) AFM surface reconstruction demonstrating roughness on the order of colloid size, and g) SEM micrographs of a silicon microgear converted by a magnesiothermic reduction of the porous silica microgear shown in (d). This conversion reaction yields the nanoporous silicon replica shown at higher magnification in (h) with (i) EDX revealing a large silicon peak. [Scalebars are 50 µm for (a,d,g), 5 µm for (b,e,h), and 500 nm for the inset in (h).]

In summary, we have patterned microcomponents with a diverse array of geometric shapes, compositions, and physical properties with overall dimensions that range from approximately $10\,\mu m$ to 1 mm at rates that exceed 10^3 min^{-1} using the SFL technique. Colloidal microcomponents may be used as novel granular media for fundamental studies of flow, packing, and compaction

© 2008 WILEY-VCH Verlag GmbH & Co. KGaA, Weinheim

behavior. Recent efforts have shown that significant packing enhancements are observed simply by changing granule shape from spherical to ellipsoidal granules.[41] Now, the possibility exists to explore such effects over a much broader range of granular shapes. Moreover, one can create granular building blocks with increasing chemical complexity by coflowing multiple suspensions of varying composition within the microfluidic device. For example, utilization of granular feedstock with Janus[29,42] or other patchy motifs[43,44] would enable the fabrication of more sophisticated bulk ceramics with nearly periodic compositional variations. We have also demonstrated that the patterned colloidal microcomponents can be converted to functional structures by densifying them at elevated temperature or via novel chemical conversion and replication schemes. As one example, porous silicon microcomponents may find potential application as gas sensors[40] photoluminescent materials[39,45] or MEMS devices. In related work, porous silicon structures replicated from biologically engineered silica "granules", or diatom frustules, have been shown to exhibit both rapid response times and high sensitivity to gases, such as nitrous oxide.[40] Finally, given their reduced contact area and weight, they should exhibit reduced *in-use* stiction[46] and require less power for actuation in MEMS applications.

Experimental

Materials System: Colloidal suspensions are prepared by first adding an appropriate amount of polyethyleneimine (PEI); (1800 g mol^{-1}); Aldrich Chemical Co to deionized water. The solution pH is then adjusted to 6 by adding aliquots of a 1M HNO_3 solution (Fisher Scientific). Following this, silica microspheres ($\phi^{v}_{silica} = 0.5$, (500 ± 25) nm diameter, FUSO, Japan) are added to the solution and allowed to stir overnight to allow the desired adsorption of (0.5 mg) PEI m^{-2} silica.[47] This opaque suspension is then index-matched by the addition of dimethyl sulfoxide (DMSO; Fisher Scientific) to achieve a volumetric ratio of 65:35 v v^{-1} DMSO to water. The suspension is then concentrated by centrifuging at 3000 rpm. After the supernatant is decanted, a photoinitiator, $\phi^{v}_{init} = 0.03$ (Darocur 1173, Ciba), acrylamide monomer, a $\phi^{w}_{acryl} = 0.09$ (Acros Organics), and crosslinking agent *N*,*N*-methylene bisacrylamide (Aldrich Chemical Co.) at an 8:2 w w^{-1} ratio of monomer to crosslinking agent is added to the dense sediment. The index-matching is finely tuned by adding deionized water to yield a final composition of $\phi^{v}_{silica} = 0.50$, 62:38 v v^{-1} of DMSO:water, and $\phi^{w}_{acrylamide} = 0.08$. Note, to facilitate direct visualization of representative patterned microcomponents, silica microspheres (ca. 700 nm in diameter) are synthesized with a fluorescent, rhodamine isothiocyanate (RITC) core-shell architecture following the procedure described in ref. [48]. A 1:9 number ratio of fluorescent to non-fluorescent silica is utilized in suspension.

Suspension Rheology: Viscometry measurements are carried out on suspensions of varying colloid volume using a controlled-stress rheometer (CVOR, Bohlin) equipped with a cup and bob geometry (C15 cell). Prior to taking measurements, a preshear of 50 s^{-1} is applied for 10 seconds and allowed to rest for 300 seconds before starting each experiment. We start with the 50 v/o suspension used in microcomponent formation, and measure the viscosity from a shear rate of 0.01 to 300 s^{-1}. After the measurement, the suspension is diluted with the acrylamide solution, and the measurement is subsequently repeated for 45, 40, and 35 v/o suspensions.

Device Fabrication: Microfluidic devices are produced via soft lithography[49] by pouring PDMS (Sylgard 184; Dow Corning) onto a silicon wafer patterned with SU-8 photoresist features (SU-8 50; Microchem). After curing the PDMS, the mold is cut out and treated via UVO[50] with an accompanying PDMS coated coverslip. After treatment, the mold and coverslip is brought into conformal contact and allowed to bond, forming a monolithic structure. Though we did not find it necessary, in most cases, to protect the microchannel surface during UVO, we still followed the protection procedures developed in ref. [1] The microchannel dimensions used in these experiments are 1 mm in diameter with channel heights of either 30 μm, 40 μm, or 55 μm, by spin-coating at either 3000, 2500, or 2000 rpm, though channel heights as low as 10 μm have been successfully used in this system. Photomasks are rendered with CAD (Autocad 2005) and printed via a high-resolution laser printer (5080 dpi; CAD/Art Services, Inc.).

Stop-Flow Lithography: The transparent colloidal suspension is flowed into the microfluidic device in a pulsed sequence and synched with flashes of UV exposure as described in ref.[33] For this material system, by applying a voltage to a solenoid valve through software written in Labview, the suspension is flowed at 2 psi for 400 ms, the pressure is then stopped by removal of the applied voltage. After the pressure is released, the system is allowed to relax for 300 ms, where the motion of the fluid comes to a full stop. Immediately after the flow is stopped, UV light is projected through a photomask into an objective lens (20 X, N.A. 0.46; Zeiss) that focuses the negative mask image onto the microchannel for a periods of 200 ms or 400 ms, depending on the reaction extent desired for polymerization and crosslinking of the acrylamide monomers. This process is repeated until the desired number of microcomponents are formed.

Particle Tracking: A concentrated colloidal suspension ($\phi_{silica} = 0.5$) that contains a dilute amount ($\phi = 0.001$) of 1.6 μm latex beads (Sulfate modified; A37297; Invitrogen) is flowed through representative microchannels that are 1 mm wide, 1 cm long, and 40 μm thick. A pressure of 2 psi is applied for 1 s and turned off for 2 s, before repeating the cycle. A high-speed camera (Phantom V7.1) is used to record video at a frame rate of 700 fps through an objective lens (60 X oil immersion; Olympus). Particle tracking algorithms developed by Crocker and Grier for IDL are used to track a single particle at the center of the microchannel, ~20 μm into the channel depth, near the output to determine the particle position within each frame. The particle velocity is determined using the forward difference method between frames.

Thermal Processing: Representative colloidal microcomponents are harvested from the SFL device, dried, and then densified on a sapphire window (Edmunds Optics) by heating at 1 °C min^{-1} to 1150 °C for varying hold times of 1, 3, or 10 h before cooling to ambient temperature at a rate of 1 °C min^{-1}. Porous and dense glass (silica) microgears are produced depending on the hold time employed. Note, dense zirconia substrates are used for samples, when substrate transparency is not required.

Silicon Replication: Porous glass microgears are transformed into silicon replicas by a magnesiothermic reduction process.[40] Each microgear is placed on a silicon substrate within a low carbon (1010) steel boat. The source of magnesium vapor, Mg_2Si powder (99.5% purity, Alfa Aesar) (0.3 g), is placed at the other end of the steel boat at a distance of 1 cm from the microgear. The steel boat is placed within a steel ampoule (2.5 cm in diameter, 15.2 cm in length) that is then welded shut in an argon atmosphere. The ampoule is heated at a rate of 7 °C min^{-1} to 850 °C and held at this temperature for 2.5 h to allow the magnesium vapor to fully react with the porous silica microgear to yield a mixture of magnesium oxide and silicon. After cooling to room temperature, the reacted gear is removed from the ampoule and then immersed in an hydrochloric acid (HCl) solution (HCl:H_2O:EtOH molar ratio of 0.7:4.7:8.9) for 4 h at room temperature to selectively dissolve MgO yielding the desired nanoporous silicon microcomponents.

Microcomponent Characterization: Representative colloidal microcomponents that contain fluorescent-core silica microspheres are harvested from the SFL device, dried, and then immersed in a

© 2008 WILEY-VCH Verlag GmbH & Co. KGaA, Weinheim

65:35 DMSO:water solution prior to imaging with a confocal scanning fluorescence microscope (SP2 Multiphoton, Leica) equipped with an Argon laser (excitation wavelength of 514 nm). Confocal *x*–*y* scans are acquired at 0.765 μm intervals in the *z*-direction through a given microcomponent. The images are then compiled into a 3D rendering using Amira imaging software and the *x*, *y*, and *z* values given from the confocal images. Representative colloidal, glass, and nanoporous silicon microcomponents are imaged using scanning electron microscopy (SEM) (6060 LV, JEOL). Energy dispersive x-ray analysis (EDX) (ISIS, Oxford Instruments) is performed on replicated silicon microgears to verify complete reaction and MgO dissolution conversion. In addition, surface roughness measurements are carried out using atomic force microscopy (AFM) (MFP-3D; Asylum Research). These data are acquired by probing three 25 μm^2 areas selected randomly. The root-mean-squared, RMS, roughness values are calculated by taking an average of each data set after applying a 3rd degree polynomial flatness convolution algorithm.

Received: April 20, 2008
Published online: November 4, 2008

[1] J. A. Lewis, *J. Am. Ceram. Soc.* **2000**, *83*, 2341.
[2] S. J. Lukasiewicz, *J. Am. Ceram. Soc.* **1989**, *72*, 617.
[3] Y. Chen, J. Au, P. Kazlas, A. Ritenour, H. Gates, M. McCreary, *Nature* **2003**, *423*, 136.
[4] F. S. Collins, V. A. McKusick, *JAMA J. Am. Med. Assoc.* **2001**, *285*, 540.
[5] P. York, P. V. Marshall, *Powder Technol.* **1993**, *74*, 171.
[6] S. A. Cryer, *AIChE J.* **1999**, *45*, 2069.
[7] A. Darelius, A. Rasmuson, I. N. Bjorn, S. Folestad, *Powder Technol.* **2005**, *160*, 209.
[8] A. D. Stroock, S. K. W. Dertinger, A. Ajdari, I. Mezic, H. A. Stone, G. M. Whitesides, *Science* **2002**, *295*, 647.
[9] D. Mundinger, R. Beach, W. Benett, R. Solarz, W. Krupke, R. Staver, D. Tuckerman, *Appl. Phys. Lett.* **1988**, *53*, 1030.
[10] G. M. Gratson, F. Garcia-Santamaria, V. Lousse, M. Xu, S. Fan, J. A. Lewis, P. V. Braun, *Adv. Mater.* **1996**, *8*, 461.
[11] O. Lehmann, M. Stuke, *Science* **1995**, *270*, 1644.
[12] R. Schuster, V. Kirchner, P. Allongue, G. Ertle, *Science* **2000**, *289*, 98.
[13] J. P. Desbiens, P. Masson, *Sens. Actuators A* **2007**, *136*, 554.
[14] R. Klajn, K. J. M. Bishop, M. Fialkowski, M. Paszewski, C. J. Campbell, T. P. Gray, B. A. Grzybowski, *Science* **2007**, *316*, 261.
[15] E. W. Becker, W. Ehrfeld, P. Hagmann, A. Maner, D. Munchmeyer, *Microelectron. Eng.* **1986**, *4*, 35.
[16] J. Hruby, *MRS Bull.* **2001**, *26*, 337.
[17] R. B. Rao, K. L. Krafcik, A. M. Morales, J. A. Lewis, *Adv. Mater.* **2005**, *17*, 289.
[18] Z. Y. Liu, N. H. Loh, S. B. Tor, K. A. Khor, Y. Murakoshi, R. Maeda, T. Shimizu, *J. Mater. Process Technol.* **2002**, *127*, 165.
[19] C. J. Campbell, S. K. Smoukov, K. J. M. Bishop, E. Baker, B. A. Grzybowski, *Adv. Mater.* **2006**, *18*, 2004.
[20] C. Provin, S. Monneret, H. Le Gall, S. Corbell, *Adv. Mater.* **2003**, *15*, 994.
[21] P. G. Conrad, II, P. T. Nishimura, D. Aherne, B. J. Schwartz, D. Wu, N. Fang, X. Zhang, M. J. Roberts, K. J. Shea, *Adv. Mater.* **2003**, *15*, 1541.
[22] G. L. Benavides, L. F. Bieg, M. P. Saavedra, E. A. Bryce, *Microsyst. Technol.* **2002**, *8*, 395.
[23] D. Dendukuri, K. Tsoi, T. A. Hatton, P. S. Doyle, *Langmuir* **2005**, *21*, 2113.
[24] S. Xu, Z. Nie, M. Seo, P. Lewis, E. Kumacheva, H. A. Stone, P. Garstecki, D. B. Weibel, I. Gitlin, G. M. Whitesides, *Angew. Chem. Int. Ed.* **2005**, *44*, 724.
[25] M. Seo, Z. Nie, S. Xu, M. Mok, P. C. Lewis, R. Graham, E. Kumacheva, *Langmuir* **2005**, *21*, 11614.
[26] K.-H. Roh, D. C. Martin, J. Lahan, *Nat. Mater.* **2006**, *4*, 759.
[27] B. De Geest, J. P. Urbanski, T. Thorsen, J. Demeester, S. C. De Smedt, *Langmuir* **2005**, *21*, 10275.
[28] W. J. Jeong, J. Y. Kim, J. Choo, E. K. Lee, C. S. Han, D. J. Beebe, G. H. Seong, H. L. Sang, *Langmuir* **2005**, *21*, 3738.
[29] R. F. Shepherd, J. C. Conrad, S. K. Rhodes, D. R. Link, M. Marquez, D. A. Weitz, J. A. Lewis, *Langmuir* **2006**, *22*, 8618.
[30] P. B. Umbanhowar, V. Prasad, D. A. Weitz, *Langmuir* **2000**, *16*, 347.
[31] T. Thorsen, R. W. Roberts, F. H. Arnold, S. R. Quake, *Phys. Rev. Lett.* **2001**, *86*, 4163.
[32] K. E. Sung, S. A. Vanapalli, D. Mukhija, H. A. McKay, J. M. Millunchick, M. A. Burns, M. J. Solomon, *J. Am. Chem. Soc.* **2008**, *130*, 1335.
[33] D. Dendukuri, S. S. Gu, D. C. Pregibon, T. A. Hatton, P. S. Doyle, *Lab Chip* **2007**, *7*, 818.
[34] C. J. Love, D. B. Wolfe, H. O. Jacobs, G. M. Whitesides, *Langmuir* **2001**, *17*, 6005.
[35] D. C. Pregibon, M. Toner, P. S. Doyle, *Science* **2007**, *315*, 1393.
[36] D. Dendukuri, T. A. Hatton, P. S. Doyle, *Langmuir* **2007**, *23*, 4669.
[37] J. Jang, D. Dendukuri, T. A. Hatton, E. L. Thomas, P. S. Doyle, *Angew. Chem. Int. Ed.* **2007**, *46*, 9027.
[38] T. Gervais, J. El-Ali, A. Günther, K. F. Jensen, *Lab Chip* **2006**, *6*, 500.
[39] L. A. Balagurov, B. M. Leiferov, E. A. Petrova, A. F. Orlov, E. M. Panasenko, *J. Appl. Phys.* **1996**, *79*, 7143.
[40] Z. Bao, M. R. Weatherspoon, S. Shian, Y. Cai, P. D. Graham, S. M. Allan, G. Ahmad, M. B. Dickerson, B. C. Church, Z. Kang, H. W. Abernathy, III, C. J. Summers, M. Liu, K. H. Sandhage, *Nature* **2007**, *446*, 172.
[41] A. Donev, I. Cisse, D. Sachs, E. A. Variana, F. H. Stillinger, R. Connelly, S. Torquato, P. M. Chaikin, *Science* **2004**, *303*, 990.
[42] Z. Nie, W. Li, M. Seo, S. Q. Xu, E. Kumacheva, *J. Am. Chem. Soc.* **2006**, *128*, 9408.
[43] S. C. Glotzer, M. J. Solomon, *Nat. Mater.* **2007**, *6*, 557.
[44] S. C. Glotzer, *Science* **2004**, *306*, 419.
[45] B. Gelloz, A. Kojima, N. Koshida, *Appl. Phys. Lett.* **2005**, *87*, 031107,1.
[46] N. Tas, T. Sonnenberg, H. Jansen, R. Legtenberg, M. Elwenspoek, *J. Micromech. Microeng.* **1996**, *6*, 385.
[47] J. E. Smay, G. M. Gratson, R. F. Shepherd, J. Cesarano, III, J. A. Lewis, *Adv. Mater.* **2002**, *14*, 1279.
[48] N. A. M. Verhaegh, A. van Blaaderen, *Langmuir* **1994**, *10*, 1427.
[49] X.-M. Zhao, Y. Xia, G. M. Whitesides, *J. Mater. Chem.* **1997**, *7*, 1069.
[50] K. Efimenko, W. E. Wallace, J. Genzer, *J. Colloid Interface Sci.* **2002**, *254*, 306.

© 2008 WILEY-VCH Verlag GmbH & Co. KGaA, Weinheim